Control of the morphology and surface properties of nickel ferrite

G. B. McGARVEY*
Atomic Energy of Canada Limited, Chalk River Laboratories, Chalk River, Ontario, Canada K0J 1J0

D. G. OWEN
Atomic Energy of Canada Limited, Whiteshell Laboratories, Pinawa, Manitoba, Canada R0E 1L0

Nickel ferrite powders with particle sizes in the 3–5 μm range have been prepared from coprecipitated nickel–iron oxalate precursors. Firing the nickel–iron oxalate precursor in the range 300–1100 °C produced samples of high chemical purity, while introducing significant variations in the distribution of crystallite sizes and surface morphologies. An increase in the powder density from 4.2 to 5.2 g cm^{-3} and a decrease in the surface area of the nickel ferrite from 120 to 0.2 m^2 g^{-1} were effected by increasing the firing temperature to 1100 °C.

1. Introduction

Transition-metal ferrites are a family of oxides that play an important role in fields as varied as corrosion [1, 2], heterogeneous catalysis [3–5] and the preparation of magnetic and electrical devices such as thermistors and recording media [6–10]. The basis for the wide range of applications is related to the variety of transition-metal cations that can be incorporated into the lattice of the parent magnetite ($Fe^{2+}Fe_2^{3+}O_4$) structure. In addition to stoichiometric substitution for the ferrous and ferric cations, non-stoichiometric materials with a range of cations, and hence chemical and physical properties, can be prepared.

In technologies where ferrites are to be used for magnetic or electrical applications, high-density materials are generally required and the ferrites are often prepared by high-temperature solid-state reactions between finely ground powders [10]. Alternatively, several coprecipitated precursor systems have been used, including oxalates [11], hydrazinates [12], and combinations of the two [7, 13]. These methods offer some advantages over the powder-based methods, including the formation of molecular precursors containing all the metal species that are desired in the final material. In addition, the temperatures required to yield the ferrite phase may be lower than those required for powder processing.

Although most applications of ferrites as ceramic materials require high densities to achieve the desired properties, there are many applications for which lower densities and high surface areas are preferred. Lower-temperature methods offer many potentially attractive features for materials synthesis, particularly when the materials are to be used as simulated corrosion products or heterogeneous catalysts. In CANDU™ (a registered trademark of Atomic Energy of Canada Limited; abbreviated from Canada deuterium uranium.) nuclear reactors, the primary heat-transport system is operated using pressurized liquid D_2O at temperatures between 250 and 300 °C under reducing conditions. Carbon steel is one of the materials used to construct the primary heat-transport circuit, and magnetite is the principal corrosion product. Corrosion of stainless steels and alloys containing constituent transition metals such as nickel, zinc, copper or chromium can lead to the formation of the corresponding stoichiometric or non-stoichiometric ferrite spinels $Ni_xFe_{3-x}O_4$, $Zn_xFe_{3-x}O_4$ and $Cu_xFe_{3-x}O_4$ or chromium-based spinels of multicomponent compositions [1, 14]. The secondary steam generator feed-water system also generates ferrite corrosion products. In this case, the temperatures can be much lower and cover a broader range (30–250 °C), but the principal oxide is magnetite. Deposits of nickel ferrite ($Ni_xFe_{3-x}O_4$, $x = 0$–1) phases have been found at some, but not all, stations that use nickel alloys for various components [15, 16]. In the primary and secondary systems, both magnetite and nickel ferrite accumulate in the steam generators and form deposits that can impede efficient heat transfer from the primary to the secondary water. In addition, the deposits, which form sludge piles around the tubes on the tube sheet, concentrate impurities from the water, producing an environment that is susceptible to under-deposit pitting corrosion.

* To whom all correspondence should be addressed.

0022–2461 *Published with permission from the Canadian Government*

Several maintenance strategies have been developed to control the detrimental effects of the accumulation of magnetite and other iron-based corrosion products, in both the primary and the secondary circuits. CANDECON™ reagents have been successfully used to dissolve some activated corrosion products in primary circuits and reduce radiation fields [17]. Chemical cleaning of the secondary side of steam generators using specially developed solvents removes the deposits and recovers some of the heat-transfer characteristics of the unit [18]. Unfortunately, the solvents that are effective for the removal of magnetite deposits (normally the component of greatest quantity) are much less effective for nickel ferrite removal. Solvents for chemical cleaning and decontamination applications are generally developed using model compounds prior to application on field samples. Hydrothermal growth of nickel ferrite under simulated operating conditions is often not practical, because of the relatively long periods of time that are required to corrode the alloy or its metallic constituents. Therefore, there is interest in preparing laboratory specimens of ferrite phases rapidly and in large quantities, while maintaining the chemical and physical properties. The present study has focused on the use of an oxalate precursor system for the preparation of nickel ferrite. The goal was to prepare high-purity nickel ferrite with different morphological characteristics.

2. Experimental procedure

The mixed-metal oxalate precursor was prepared by adding a 400 cm^3 (N_2-purged) solution containing $NiSO_4 \cdot 6H_2O$ (37.54 g (0.143 mol)) and $FeSO_4 \cdot 7H_2O$ (85.49 g (0.307 mol)) to a 1000 cm^3 (N_2-purged) solution of ammonium oxalate ($(COONH_4)_2 \cdot H_2O$) (45.81 g (0.322 mol)) with vigorous stirring. Following the addition, a yellow–green suspension formed, which was chilled and partially decanted prior to filtering the solid. The precipitate was washed with distilled water and allowed to dry in air before grinding. Formation of the nickel ferrite phase was achieved by heating the precursor in air in a pre-heated muffle furnace for 1 h. Firing was carried out at 300, 495, 693, 902 and 1100 °C in alumina crucibles.

Powder X-ray diffraction (XRD) patterns were recorded on a Rigaku Rotaflex diffractometer using Cu Kα radiation. The lattice parameter or lattice dimension, a_0, for the cubic spinel phase was determined using the Nelson–Riley extrapolation method [19]. Scanning electron microscopy (SEM) images were measured using an ISI DS-130 instrument. Density measurements were made using carbon tetrachloride as the displacement fluid. Nitrogen adsorption isotherms were measured at 77 K using a volumetric gas adsorption system and nitrogen as the adsorbate, with subsequent surface-area determinations being made using the Brunauer–Emmett–Teller [20] theory. Infrared spectra were recorded on a Bomem DA3 Fourier transform spectrometer. Nickel and iron were analysed using inductively coupled plasma spectrometry after the samples had been fused in a lithium borate flux and subsequently dissolved. Carbon analyses were performed by determining the volume of carbon dioxide evolved during the combustion of the sample in the Leco induction furnace.

3. Results and discussion

The nickel–iron oxalate precursor was a yellowish-green powder. Powder XRD indicated that the precursor was crystalline and possessed a layered type of lattice. The principal interplanar *d*-spacing values listed in Table I are in good agreement with those reported previously for a series of nickel–iron oxalates [21]. No evidence for significant formation of impurity phases was evident from the powder XRD pattern. Consistent with the presence of the oxalate moiety, stretching and bending bands for symmetric (1317 and 1362 cm^{-1}) and asymmetric (1636 cm^{-1}) O–C–O stretches, C = C–O bending (821 cm^{-1}) and O–C–O bending (493 cm^{-1}) were observed [7, 13]. Chemical analyses confirmed a significant quantity of carbon in the precursor and also confirmed the target Ni : Fe ratio of 1 : 2. Fig. 1 shows a scanning electron micrograph of the nickel–iron oxalate precursor particles prior to heating. Note the plate-like structure mentioned previously for the precursor, and the distribution of particles in the 5–20 μm range. The morphology of this nickel–iron oxalate is similar to that which was recently shown for a more complex manganese–nickel–iron formulation [6].

In order to determine the effect of time on the decomposition of the nickel–iron oxalate precursor to nickel ferrite, samples were heated for 0.5, 1.0, 2.0 and

TABLE I Principal interplanar spacings and relative intensities for a nickel–iron oxalate complex

Diffraction angle 2θ (deg)	Interplanar spacing (nm)	I/I_0 (%)
18.39	0.4821	100
22.89	0.4213	16.2
29.11	0.3065	14.7
34.66	0.2586	10.3
42.96	0.2104	7.6
45.91	0.1975	4.8
48.37	0.1880	7.1

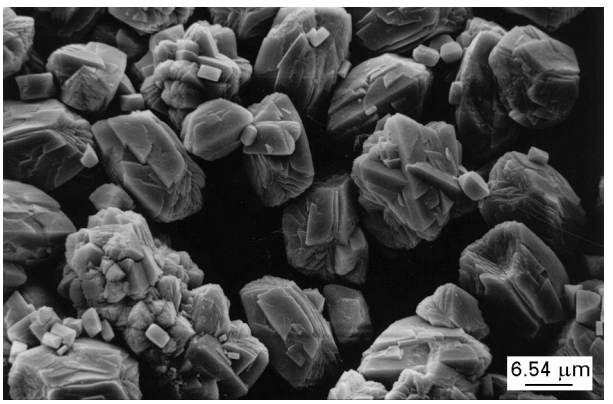

Figure 1 SEM images of a nickel–iron oxalate powder.

24 h at 902 °C. SEM and powder XRD studies indicated that the decomposition to nickel ferrite did not change significantly over the range of reaction times, and that the differences in crystallinity were minimal. Subsequent experiments carried out using different temperatures were performed using a 1 h heating period.

The effect of decomposition temperature on the morphology and crystallinity of the nickel ferrite that was produced in the reaction was significant. Fig. 2 shows the powder XRD patterns that were recorded for the samples prepared between 300 and 1100 °C. Nickel ferrite was identified as the major, and in most cases only, crystalline decomposition product at each temperature. Trace quantities of haematite were detected following firing at 693 and 902 °C. It is evident that there was an evolution in the crystallinity of the nickel ferrite as the temperature increased. Substantial narrowing of the peaks was observed, particularly when the temperature was increased from 300 to 495 °C. The peak widths approached what appeared to be a limiting value for this thermal treatment duration (1 h) as the temperature was increased further to 693 °C and higher. Fig. 3 shows how six of the major diffraction peaks of nickel ferrite narrowed and reached a limiting width of approximately 0.16 ° (2θ).

Table II lists lattice parameters for the nickel ferrite samples. Temperature did not have a significant influence on the value of a_0, indicating that it did not greatly influence the incorporation or diffusion of the nickel and iron into the spinel lattice. Further, this suggests that Ni and Fe were homogeneously distributed in the oxalate precursor.

Figs 4 and 5 show representative scanning electron micrographs of nickel ferrite prepared at different temperatures. Heating in air at 300 and 495 °C altered the particle-size range from that of the precursor to approximately 3–8 μm for both temperatures; in addition, microstructural changes occurred that were detectable using SEM. The particles lose the sharp edges and definition at temperatures as low as 300 °C (Fig. 4a), and at 495 °C (Fig. 4b) significant microstructural changes occurred. In addition to some delamination, close examination of the particle surfaces generated at 495 °C shows the development of additional texture. The appearance of roughness on the surface is attributed to crystal growth of the nickel ferrite within the large particles.

The textural evolution continued as the temperature for the conversion of the nickel–iron oxalate precursor to nickel ferrite was increased. At 693 °C, the individual nickel ferrite crystallites were more apparent (Fig. 5a). The smaller crystallites that had evolved as part of the larger particles adopted particle sizes in the 1–4 μm range. When the temperature was increased to 902 °C, discrete crystals on the surface of the larger agglomerates were readily observed (Fig. 5b). The nickel ferrite crystallites were approximately 0.5–1 μm in diameter. Increasing the temperature to 1100 °C resulted in some loss of distinction of the individual crystallites, presumably because the sample had undergone a degree of sintering (Fig. 5c and d).

The micrographs in Fig. 5 show that, as the temperature was raised above 700 °C, the distinctive shape of the large precursor and nickel ferrite particles prepared at lower temperatures changed radically; the particle size decreased and individual crystallites became more prevalent as the void space was eliminated. The microscopy observations were confirmed by measuring the density and surface areas of the materials as a function of temperature (Table III). As the temperature was increased from 300 to 1100 °C, there was a progressive increase in the density of the nickel ferrite from 4.2 to 5.2 (Table III). The measured density of 5.2 obtained at 1100 °C approaches the reported theoretical density of 5.37 for nickel ferrite (96.8% of the theoretical density) [22]. The

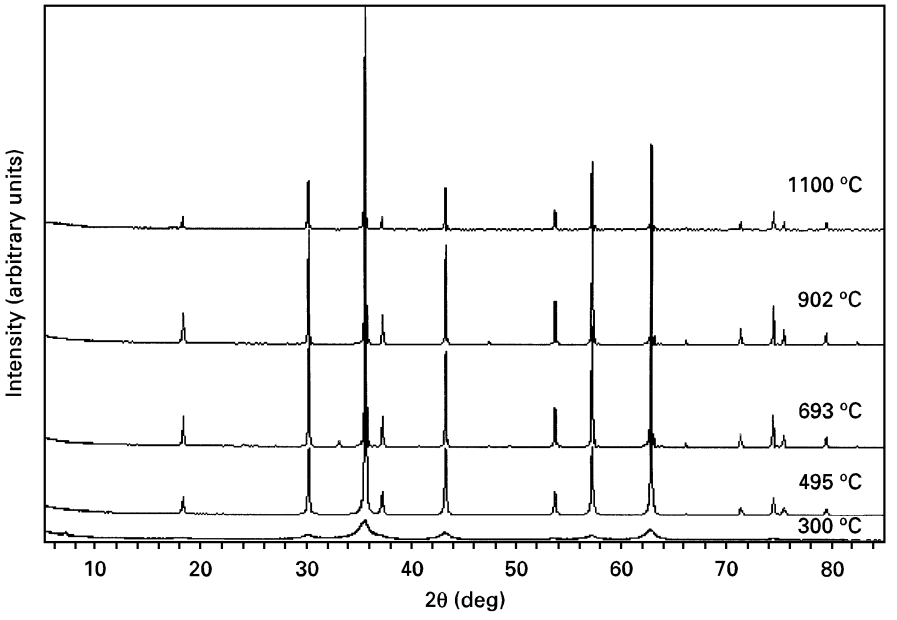

Figure 2 Powder XRD patterns of nickel ferrite prepared at several different firing temperatures.

micrographs of the nickel ferrite prepared at 1100 °C (Fig. 5c and d) showed that some void space remains between crystallites in the material, and it has been reported that sintering temperatures of 1400 °C are required to achieve the theoretical density [23]. Surface areas of nickel ferrite samples are also listed in Table III. The change in the surface area as a function of heating temperature was consistent with the increase in density and a loss of bulk porosity. Transition-metal ferrites crystallize as discrete individual particles and do not possess an intrinsic pore network such as that found in aluminosilicates. The high surface area that was measured for the sample heated at 300 °C is attributed to the significant void space between individual crystallites in the lower-density material. Again, the SEM images in Fig. 4 are a good representation of the more open structure of the materials prepared at lower temperatures, compared with the materials prepared at higher temperatures.

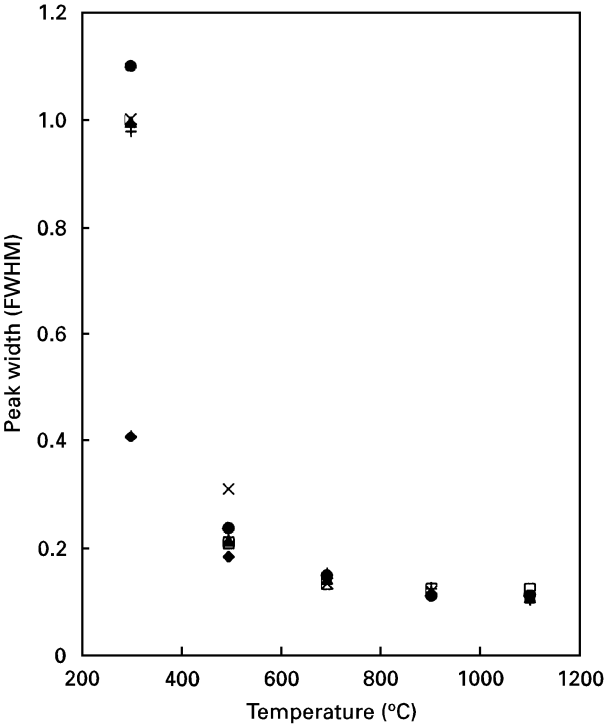

Figure 3 Plot of the variation in powder XRD peak widths (full widths at half-maximum ($FWHM_5$)) for nickel ferrite prepared at different temperatures. (◆), 1 1 1; (□), 2 2 0; (×), 3 1 1; (+), 4 0 0; (▲), 5 1 1; (●), 4 4 0.

TABLE II Lattice parameters for nickel ferrite prepared from nickel–iron oxalate precursors at different temperatures

Temperature (°C)	Lattice parameter (nm)
300	0.8332
495	0.8337
693	0.8338
902	0.8337
1100	0.8337

Fig. 6a shows the microstructure of a sintered nickel ferrite disc (1160 °C for 2 h) that was prepared using a two-step process: formation of nickel ferrite powder by decomposing the nickel–iron oxalate precursor at 495 °C for 1 h, followed by preparation and sintering of the pressed pellet. The grain sizes are in the range 1–8 μm, and there is essentially no microscopic evidence of the existence of pores at any of the grain junctions. A disc was fractured and the morphology was examined along the resulting fracture face (Fig. 6b). As was observed for the nickel ferrite powders, there is little evidence of residual porosity in the sintered body, and many individual crystallites show evidence of spinel law twinning (Fig. 6b). This demonstrates that the nickel ferrite prepared by intermediate-temperature firing can be used directly for the preparation of good-quality sintered bodies, with possible applications as electrodes for electrochemical dissolution studies or electrocatalytic reactions, as have been carried out previously on magnetite discs [24, 25].

The results reported here for the preparation of nickel ferrite from a nickel–iron oxalate precursor clearly demonstrate that the morphology, density and porosity can be systematically varied in this family of materials. While obtaining materials that approach the theoretical density is a critical component for ceramics technologies, other industries and technologies can benefit from the use of less-dense materials

Figure 4 SEM images of nickel ferrite prepared at (a) 300 °C and (b) 495 °C.

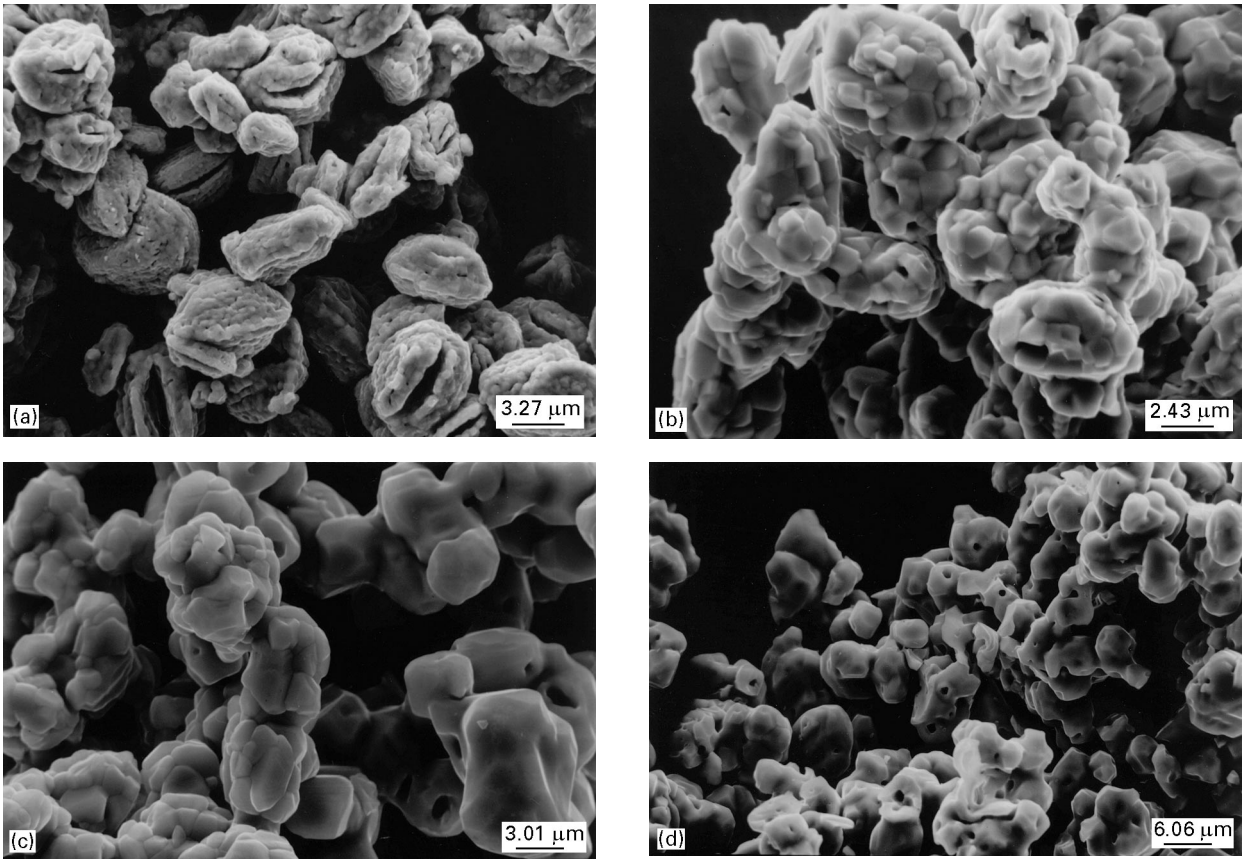

Figure 5 SEM images of the morphological evolution of nickel ferrite prepared at (a) 693 °C, (b) 902 °C and (c) and (d) 1100 °C.

TABLE III Densities and surface areas for nickel ferrite samples prepared from nickel–iron oxalate precursors at different temperatures

Temperature[a] (°C)	Density (g cm^{-3})	Surface area (m^2 g)$^{-1}$
300	4.2	120
495	4.9	9.6
693	5.0	ND[b]
902	ND[b]	1.3
1100	5.2	0.2

[a] Specimens were heated for 1 h at the indicated temperature.
[b] ND., not determined.

with more open structures. For example, the morphological and surface properties of solid materials are important features that must be considered when assessing their application in heterogeneous catalytic processes. In order to increase the number of active surface sites that are available to participate in gas–solid reactions, low-surface-area materials such as spinels are often supported on high-surface-area supports. The results obtained in this study suggest that the properties of nickel ferrite catalysts, and possibly other ferrites prepared using analogous oxalate precursors, can be tailored by the selection of the firing temperature. The ranges of morphologies, densities and surface areas that were obtained in this study suggest that it may be possible to optimize the structural features of the catalyst, particularly

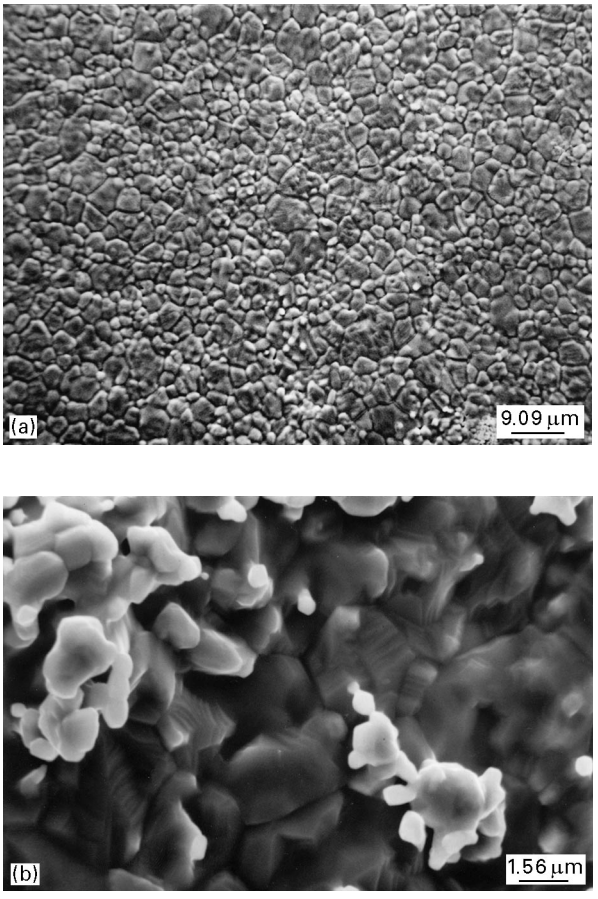

Figure 6 SEM images of the morphology of a sintered disc of nickel ferrite prepared at 1160 °C: (a) the exposed surface following firing; (b) the surface of a freshly fractured disc.

if the reaction of interest can be catalysed at temperatures below the firing temperature. Decomposition of the greenhouse gas carbon dioxide has been demonstrated at 300 °C [4]; it is an example of a process that is catalysed on nickel-ferrite-based catalysts and may benefit from modification of the surface properties and morphology by altering the mass transfer of reactants and products to and from the surface.

A second application of synthetic nickel ferrite is as a model compound for chemical dissolution studies. The difficulties associated with removing nickel ferrite deposits from primary and secondary heat-transport systems in nuclear reactors are well documented [2, 23, 26]. Fundamental to the development of effective solvents is the ability to determine the role played by the morphology and physical and chemical characteristics of the nickel ferrite samples that are used in the testing. Segal and Sellers [23] have investigated reductive dissolution of nickel ferrite using low-oxidation-state metal ion reagents such as vanadium(II) picolinate. The studies were carried out on a series of nickel ferrite samples that were prepared using high-temperature calcining methods. They found that raising the calcination temperature from 1000 to 1400 °C decreased the dissolution rate constant. They were unable, however, to study nickel ferrite that was prepared at lower temperatures, because of the high levels of haematite that were formed as byproducts of their reaction. Using the results obtained in this work, it must therefore be assumed that the densities of their samples were all close to the theoretical density. While this may be valid for some deposits that are found in the primary heat-transport systems, the lower temperatures of the secondary feed-water system may result in lower-density deposits. The intermediate-temperature firing of the readily decomposed nickel–iron oxalate precursor can yield nickel ferrite with densities in the range 4.2–5.2 which is likely to influence the ability of the solvents to penetrate into and out of deposits.

4. Conclusions

Thermal decomposition of a nickel–iron oxalate precursor was found to be an effective method for preparing stoichiometric nickel ferrite of high chemical purity. Changing the temperature for the decomposition of the precursor had a significant impact on the morphology, density and porosity of the nickel ferrite particle agglomerates. Evidence obtained from powder XRD measurements indicated that the firing temperature did not significantly influence the distribution or diffusion of the nickel and iron in the spinel lattice. The material that was prepared at 495 °C was found to be an effective intermediate for the preparation of sintered discs of nickel ferrite.

Acknowledgements

We thank D. Doern for measuring the powder XRD patterns, and A. M. Hearn for measuring the surface areas. This work was funded by the Atomic Energy of Canada Limited Underlying Chemistry Program.

References

1. T. E. RUMMERY, J. J. HAWTON and D. OWEN, *Corrosion* **33** (1977) 369.
2. J. Y. CHUNG and K. J. LEE, *High Temp. Sci.* **30** (1990) 51.
3. P. LAHIRI and S. K. SENGUPTA, *J. Chem. Soc., Faraday Trans.* **91** (1995) 3489.
4. M. TSUJI, H. KATO, T. KODAMA, S. CHANG, N. HESEGAWA and Y. TAMAURA, *J. Mater. Sci.* **29** (1994) 6227.
5. M. DO CARMO RANGEL, R. M. SASSAKI and F. GALEMBECK, *Catal. Lett.* **33** (1995) 237.
6. Y. TORII, A. TSUZIKI, K. KATO, Y. UWAMINO, B. H. CHOI and M. J. LEE, *J. Mater. Sci.* **31** (1996) 2603.
7. V. MOYE, K. S. RANE and V. N. KAMAT DALAL, *J. Mater. Sci.: Mater. Electr.* **1** (1990) 212.
8. E. UZUNOVA, D. KLISSURSKI and S. KASSABOV, *J. Mater. Chem.* **4** (1994) 153.
9. K. SAJATA and T. O. MASON, *J. Amer. Ceram. Soc.* **75** (1992) 557.
10. F. NOVELO and R. VALENZUELA, *Mater. Res. Bull.* **30** (1995) 335.
11. L. FA-SHEN, Y. DE-SHENG, Z. HUA-XIN, L. XIN-FEN and Y. ZHENG, *Hyperfine Interactions*, **41** (1988) 525.
12. K. SURESH and K. C. PATIL, *J. Solid State Chem.* **99** (1992) 12.
13. D. GAJAPATHY and K. C. PATIL, *Mater. Chem. Phys.* **9** (1983) 423.
14. T. E. RUMMERY and D. D. MACDONALD, *J. Nucl. Mater.* **55** (1975) 23.
15. F. GONZALEZ, J. M. T. RAYCHEBA and P. SPEKKENS, in 'Proceedings of the Second International Symposium on the Environmental Degradation of Materials in Nuclear Reactors' (American Nuclear Society, Lagrange Park, Ill 1986) p. 539.
16. R. L. TAPPING, C. W. TURNER, R. H. THOMPSON and R. H. THOMPSON, *Corrosion* **47** (1991) 489.
17. R. A. SPERANZINI, R. VOIT and M. HELMS, *Nucl. Engng. Int.* **53** (1990) 52.
18. P. V. BALAKRISHNAN, P. McSWEENY, C. R. FROST and P. WALMSLEY, *Nucl. Technol.* **55** (1981) 349.
19. E. W. NUFFIELD, "X-ray Diffraction Methods" (J. Wiley, New York, 1966) p. 157.
20. S. BRUNAUER, P. H. EMMETT and E. TELLER, *J. Amer. Chem. Soc.* **60** (1938) 309.
21. W. J. SCHEULE and V. D. DEETSCREEK, in "Ultrafine Particles", edited by W. E. Kuhn (J Wiley, New York, 1963), p. 218.
22. C. R. WEAST, (ed.), in "Handbook of Chemistry and Physics", 50th Edn (Chemical Rubber Company, Cleveland, OH, 1969) p. B232.
23. M. G. SEGAL and R. M. SELLERS, *J. Chem. Soc., Faraday Trans. I* **78** (1982) 1149.
24. R. I. HAINES and D. G. OWEN, *J. Phys. Chem. Solids* **47** (1986) 647.
25. E. R. VAGO, E. J. CALVO and M. STRATMANN, *Electrochimica Acta* **39** (1994) 1655.
26. Y. NISHINO, Y. ASAKURA, T. SAWA, S. UCHIDA, K. OHSUMI, S. YOSIKAWA, O. AMANO and N. SUZUKI, *J. Nucl. Sci. Technol.* **28** (1991) 848.

Received 12 February
and accepted 30 July 1997